2013-08

Optimal Trajectory Generation and Tracking Control of a Single Coaxial Rotor UAV

Bollino, Kevin; Harada, Masanori; Nagata, Hideyuki; Simond, Johan

American Institute of Aeronautics and Astronautics, Inc

Guidance, Navigation, and Control and Co-located Conferences August 19-22, 2013, Boston, MA AIAA Guidance, Navigation, and Control (GNC) Conference
http://hdl.handle.net/10945/48626

Guidance, Navigation, and Control and Co-located Conferences
August 19-22, 2013, Boston, MA
AIAA Guidance, Navigation, and Control (GNC) Conference

Optimal Trajectory Generation and Tracking Control of a Single Coaxial Rotor UAV

Masanori Harada*, Hideyuki Nagata†
National Defense Academy of Japan
1-10-20 Hashirimizu, Yokosuka 239-8686, Japan

and

Johan Simond‡, *École de Saint-Cyr Coëtqudan*
56381 Guer Cedex, France

and

Kevin Bollino§
Naval Postgraduate School, Monterey, CA, 93943

This paper investigates the application of optimal control to the experimental flight of a Single Coaxial Rotor (SCR) Unmanned Aerial Vehicle (UAV) conducted in the indoor flight facility of the National Defense Academy (NDA) of Japan. The optimal control problem is prescribed as a minimum-length obstacle avoidance maneuver of the SCR UAV and it is solved using pseudospectral (PS) optimal control theory. The optimal trajectory is computed offline as a kinematic path-planning problem and then provided to the real UAV system as reference input commands. While only preliminary studies have been conducted at NDA, the results provide nominal tracking performance and validate the feasibility of the approach.

I. Introduction

Primarily due to the need to fulfill missions requiring flight at low altitudes in cluttered environments, the past few years have been marked by an increase in research related to rotorcraft unmanned aerial vehicles (UAVs).[1–12] It is no surprise that rotor UAVs offer the advantage of slow, low, hovering flight to include vertical takeoff and landing, but they are also ideal test platforms for constrained operating environements such as university reserch laboratories. For an investigator, this also offers the advantage of a better controlled environment when performing experiments.[4,11–13]

Due to their ability to hover, traverse slowly, overall manueverability, or ease of take off and landing, this kind of vehicle is well suited to follow a specified, pre-planned or online adaptive, path in a complex environment. Unfortunately, rotor UAVs and especially small rotor UAVs have the disadvantage of limited payload capability. Because of endurance limitations and as some UAV missions may require the capability to rapidly cross an area, it is important that the flight route be as short as possible. In order to minimize the distance it takes to navigate terrain while avoiding obstacles, applying optimal control theory to improve mission performance is the perfect candidate[14,15]

There have been substantial developments in numerical optimization methods for the purpose of obtaining optimal control trajectories.[16–19] The literature also includes several methods for updating the optimal control solution in real-time during maneuvers.[20,21] Although current research efforts continue to address

*Associate Professor, Department of Mechanical Engineering, AIAA Senior Member.
†Graduate Student, Mechanical Engineering.
‡Second Lieutenant, CBA BULLE Class.
§Research Associate, Department of Mechanical and Astronautical Engineering, AIAA Senior Member.

the problem of computational efficiency, the growing need for rapid calculations in trajectory optimization is fueling more practical approaches. One such approach is to compute the optimal maneuver offline and then use this reference trajectory as input commands for the feedback controller.[22] This is not a new approach and has been experimetally demonstrated to verify the adaptability of offline optimal solutions to the real flight problems. For example, a historical flight experiment for the minimum time-to-climb of the jet fighter was performed in 1962.[23] Research groups conducted flight experiments using both aircraft and helicopters to confirm the effectiveness of using offline optimal solutions.[24–26] Similar approaches have been succesfully demonstrated for space vehicle manuevers such as the Zero Propellant Maneuver (ZMP)[27,28] of the International Space Station (ISS) and the design and flight implementation of time-optimal attitude maneuvers performed onboard NASA's Transition Region and Coronal Explorer spacecraft.[29] In both of these examples, the optimal manuevers were designed and implemented using pseudospectral optimal control.[18] For this paper, we investigated adaptability of the optimal control law to the minimum-time maneuver of a Single Coaxial Rotor (SCR) UAV in the context of a feedforward control.[11]

Motivated by previous research efforts, this work investigates the use of pseudospectral (PS) optimal control theory to find optimal trajectories in a three-dimensional environment. The ability to manuever efficiently in a cluttered environment while avoiding obstacles is a highly desired attribute. Initial simulation work employing PS optimal control specifically for minimum-time obstacle avoidance began in 2006[30,31] and was later extended to include real-time information updates[32] and multiple vehicles.[33] Similar to the experiement of Karpenko et. al. in Ref.6, the focus of our work here is on the development and implementaion of a nonlinear, optimal guidance controller applied to the semi-autonomous flight of the SCR UAV.

II. Optimal trajectory generation and tracking control

The objective of this work is to adopt recent developments in the areas of optimal trajectory generation and tracking control with specific implementation to a SCR UAV in a cluttered environment. Although the ultimate goal is to form a practical (in terms of ease of implementation and computational efficiency), near-optimal, robust, integrated guidance and control architecture, the stepping-stone approach taken here pursues a combination of three separately developed methods: (1) optimal trajectory generation via kinematic path planning, (2) guidance command generation based on proportional-integral-derivative (PID)-loop closure, and (3) inner-loop tracking control.

As described in the appendix, the nonlinear dynamical model has state vector $\boldsymbol{X}(t) \in \mathbb{R}^{18}$ and control vector $\boldsymbol{U}(t) \in \mathbb{R}^4$. To simplify notation and reduce the order of the system, we only consider the kinematic equations of motion for now.

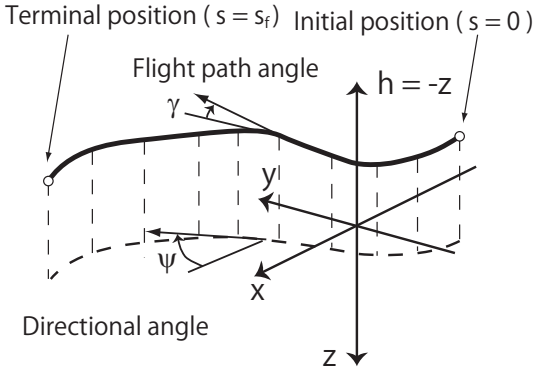

Figure 1. Coordinate system for simple kinematic path-planning model.

II.A. Kinematic model

The coordinate system for a simple kinematic path-planning model is shown in Fig.1. This nonlinear model is based on an under-actuated rigid body. The initial goal for the kinematic model is to start out simple, since it has to be used for the optimal control design including all requirements for generating a reference flight-path trajectory.

The vehicle is controlled through a longitudinal cyclic stick and anti-torque pedals. The direction of the lift is so controlled by titling forward or back through the rate of curvature u_H while the rate of curvature

u_V has an effect on the yaw rate. The state vector is $\boldsymbol{X} = [k_V\ k_H\ \gamma\ \psi\ x\ y\ h]^T \in \mathbb{R}^7$, and the control vector is $\boldsymbol{U} = [u_V\ u_H]^T \in \mathbb{R}^2$. For the three spatial degrees of freedom, (x, y) are the horizontal coordinates of the center of mass and h is the altitude. The rates of curvature are given by k_V and k_H. The additional two kinematic states are the directional angle ψ and the flight path angle γ which are related to the previous states. The directional angle is measured from a reference heading to the velocity vector, and the flight path angle is measured from the local horizontal to the velocity vector. All these characterizations result in a nonlinear kinematic model shown in Eq.(1). The independent variable station $s \in [0, s_f]$ is defined to describe location on the path.[19]

$$\dot{\boldsymbol{X}}(s) = \begin{bmatrix} \frac{dk_V}{ds} \\ \frac{dk_H}{ds} \\ \frac{d\gamma}{ds} \\ \frac{d\psi}{ds} \\ \frac{dx}{ds} \\ \frac{dy}{ds} \\ \frac{dh}{ds} \end{bmatrix} = \boldsymbol{f}[\boldsymbol{X}(s), \boldsymbol{U}(s)] = \begin{bmatrix} u_V \\ u_H \\ k_V \\ k_H \\ \cos\gamma\cos\psi \\ \cos\gamma\sin\psi \\ \sin\gamma \end{bmatrix} \tag{1}$$

II.B. Boundary constraints

In Eq.(2), the initial condition and the endpoint condition include constraints on the position and orientation, whereas both curvature k_V and k_H are unconstrained.

$$\boldsymbol{e}(\boldsymbol{x}_0, \boldsymbol{x}_f) = \begin{bmatrix} \gamma(0) - \gamma_0 \\ \psi(0) - \psi_0 \\ x(0) - x_0 \\ y(0) - y_0 \\ h(0) - h_0 \\ \gamma(s_f) - \gamma_f \\ \psi(s_f) - \psi_f \\ x(s_f) - x_f \\ y(s_f) - y_f \\ h(s_f) - h_f \end{bmatrix} = \boldsymbol{0} \tag{2}$$

II.C. Obstacle representation

Based on the premise of *a priori* landscape knoweldge, obstacles and areas with different surface are represented by primitive forms thanks to the L^p-norm.[33] In finite dimensions, the L^p-norm of x is defined by Eq.(3)

$$For\ p \geq 1, ||x||_p \quad = \quad \left(\sum_{i=1}^{n} |x_i|^p \right)^{1/p}. \tag{3}$$

In practice, only three of the L^p-norms are used, and they are the grid norm, the Euclidean norm and the max norm. The ellipse and rectangle are extensions of the circle and the square, respectively, where the distance with the center between x and y is not the same. In $\mathbb{R}^3$, the 1-, 2- and ∞-spheres are an octahedron, a ball, and a cube, respectively. In addition to this, we can easily build infinite cylinders, (or rectangles) by omitting a variable. All these basic geometries can model various shapes and represent a rudamentary

city environment. Indeed these basic geometries are all that is needed since any obstacle can be modeled by fitting one of those shapes around it. As such, an obstacle can so be represented by the following function, Eq.(4).

$$g(x,y,h) = \left|\left(\frac{x-x_c}{a}\right)^p\right| + \left|\left(\frac{y-y_c}{b}\right)^p\right| + \left|\left(\frac{h-h_c}{c}\right)^p\right| - |R^p| \qquad p \in 2n; n \in [1,50] \tag{4}$$

Where the center is (x_c, y_c, h_c), the radius r and the parameters a, b, c are used to change the scale of the axes. In order to obtain a continuous function, p is limited to the even numbers. Moreover, as $p = \infty$ cannot be computationally solved, it is fixed that $p = 100$ for the max norm. The path constraint is defined as $g_i(x, y, h) \geq 0$. Indeed, the convex equation is then used as an inequality constraint so as to define an authorized area around the obstacle. Notice that the intersection of many convex sets is itself a convex set. Instead of using a penalty function method by adding a term to the cost function, the avoidance of an obstacle is simplified by using a radius greater than the radius of the obstacle. The radius R considered in the obstacle representation is to allow an additional safety buffer zone around the obstacle.

II.D. Optimal control problem

In many problems, the performance index of interest is the elapsed time to transfer the system from its initial state to a specified terminal state. In this research, we set the cost function to minimize the distance,Eq.(5). The minimum-length problem is to find a particular trajectory which gives the smallest value for the cost, and that enables the UAV to fly from some initial condition to some final condition while satisfying the kinematic and path constraints.

$$\begin{aligned} J[\boldsymbol{X}(\cdot), \boldsymbol{U}(\cdot), s_f] &= E[X(s_f), s_f] + \int_0^{s_f} F[\boldsymbol{X}(s), \boldsymbol{U}(s)]ds \\ &= s_f \end{aligned} \tag{5}$$

From these assumptions, the optimal control problem (B) can be constructed to minimize the function J as follows.

$$(B) \begin{cases} \text{Minimize} & J[\boldsymbol{X}(\cdot), \boldsymbol{U}(\cdot), s_f] = s_f \\ \text{Subject to} & Eq.(1) \\ & Eq.(2) \\ & \boldsymbol{g}_i(\boldsymbol{X}, \boldsymbol{U}) \geq 0 \end{cases}$$

Path constraints, i.e., constraints that apply at intermediate points or over the whole path rather than just at the endpoints allow to hold a reference altitude or to account for obstacles.

II.E. Tracking control

II.E.1. Reference trajectory for tracking control

Let us begin with the optimal solution given by the optimal control solver and remember that the problem was solved by considering the station s and not the time t. Because the vehicle is required to track a time parameterized reference for the trajectory tracking, it is necessary to obtain states which depend on time. In order to work such a problem, interpolation method uses data points previously found, extends the trend to a specified maximal time t_f and then finds values at intermediate points, of a one-dimensional function that underlies the data,Eq.(6),(7). Keeping in mind that solution nodes are linked to the smooth function, it should be clear that whichever the maximal time the optimal trajectory will be exactly the same.

$$s \in [0, s_f] \mapsto t \in [0, t_f] \tag{6}$$

$$\boldsymbol{X}(s) \mapsto \boldsymbol{X}(t) \tag{7}$$

II.E.2. PID control

Although there are many path-following methods,[34] some more elaborate than others, for the purpose of simplicity we use a standard PID control for this tracking control demonstration. Referring to the nonlinear

dynamical model in the appendix, the control variables $\delta_x, \delta_y, \delta_z$ and δ_ψ of the SCR UAV can be obtained from the state variables. Note that position variables have been transformed from the inertial frame to the body-fixed reference frame thanks to Eq.(8).

$$\begin{bmatrix} x_B - x_{Bc} \\ y_B - y_{Bc} \end{bmatrix} = \begin{bmatrix} \cos\psi & \sin\psi \\ -\sin\psi & \cos\psi \end{bmatrix} \begin{bmatrix} x - x_c \\ y - y_c \end{bmatrix} \tag{8}$$

$$\delta_x = K_{Px}(x_B - x_{Bc}) + K_{Ix}\int_0^t (x_B - x_{Bc})d\tau + K_{Dx}(v_{Bx} - v_{Bxc}) + K_{P\theta}(\theta - \theta_c) + K_{D\theta}(q - q_c) \tag{9}$$

$$\delta_y = K_{Py}(y_B - y_{Bc}) + K_{Iy}\int_0^t (y_B - y_{Bc})d\tau + K_{Dy}(v_{By} - v_{Byc}) + K_{P\phi}(\phi - \phi_c) + K_{D\phi}(p - p_c) \tag{10}$$

$$\delta_z = K_{Pz}(z - z_c) + K_{Iz}\int_0^t (z - z_c)d\tau + K_{Dz}(v_z - v_{zc}) \tag{11}$$

$$\delta_\psi = K_{P\psi}(\psi - \psi_c) + K_{I\psi}\int_0^t (\psi - \psi_c)d\tau + K_{D\psi}(r - r_c) \tag{12}$$

The feedback gains were tuned by trial-and-error based on real flight maneuvers. Even for the indoor flight facility with negligible wind disturbance, the UAV's attitude varies due to the inherent feature of its nonlinear dynamics. The position error is approximately ± 0.1 m and the velocity errors are approximately ± 0.1 m/s for each x and y directions during the hovering flight.[11]

III. Numerical Simulation

Parameters for the following simulations are estimated by an unscented Kalman filter (UKF)[35,36] using flight data, Table 1.

Table 1. Single Coaxial Rotor UAV dynamic parameters.

Parameter	Unit	Value
m	kg	0.190
z_{HU}, z_{HL}	m	0.110, 0.043
J_x, J_y,J_z	kg·m^2	3.3014×10^{-4}, 5.9557×10^{-4}, 3.5009×10^{-4}
k_f	N·s^2/rad^2	2.9396×10^{-5}
k_m	N·m·s^2/rad^2	6.5185×10^{-7}
T_S	s	0.5
k_S	-	1.4319
$T_M(=1/m_3)$	s	0.045
$k_z(=m_1/T_M)$	rad/s	18.0
$k_p(=m_2/T_M)$	rad/s	1.1671
T_{fL}	s	0.2198
k_r	rad	0.5

The optimal control problem is solved by a modified method based on a Jacobi pseudospectral (PS) collocation technique.[37] Optimality of the solutions is verified by ensuring that the Hamiltonian conditions are satisfied,[18] but omitted here for brevity.

For this preliminary experiment, the environment model we use for simulations in this initial work is based on a simple cylindrical obstacle. The situation is sketched in Fig.2. For more clarity, the augmented obstacle is represented by the red circle in Fig.3. The initial location of the SCR UAV is $[x(0), y(0), h(0)] = [-0.6, -0.6, 0.7]m$, and the desired final location is specified as $[x(t_f), y(t_f), h(t_f)] = [0.6, 0.6, 0.7]m$, hovering at the boundary points. We assume for the example used in this simulation that the maximal time is $t_f = 15$ [s].

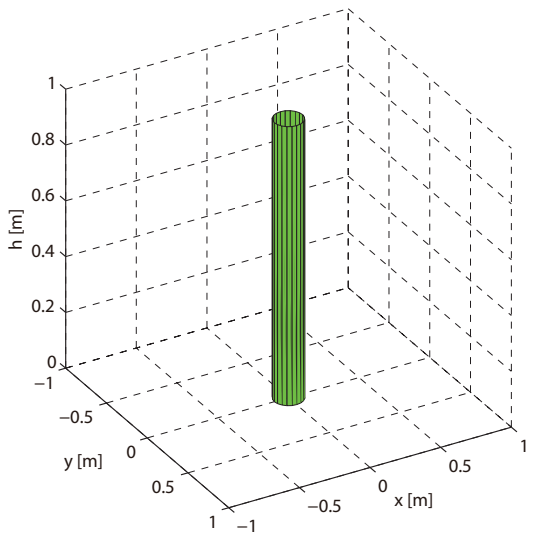

Figure 2. Obstacle representation in 3D.

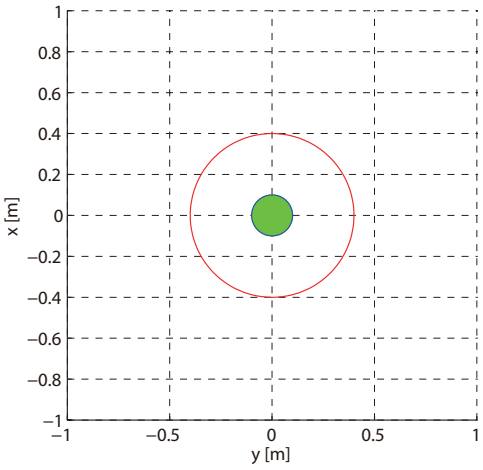

Figure 3. Obstacle representation in x-y plane.

III.A. Nose direction following tangential direction command

It is interesting to see that the use of the previous reference values is not restricted to helicopter motion. Keep in mind that the solution given by the PS solver and, specifically, the kinematic model and problem formulation described in section II is not limited to a rotor UAV, but rather is a general path planning scheme that potentially any UAV could track. For instance, a fixed-wing UAV is able to track the optimal path shown in Eq.(13) as the lateral velocity is equal to zero and the aircraft nose is following the path. The result from this simulation case is shown in Fig.4. The desired path is represented in red whereas the simulation result is in blue.

$$\begin{cases} x(t) & = & x_{cmd} \\ y(t) & = & y_{cmd} \\ \psi(t) & = & \psi_{cmd} \\ v_{Bx}(t) & = & \dfrac{s_f}{t_f} \\ v_{By}(t) & = & 0 \end{cases} \tag{13}$$

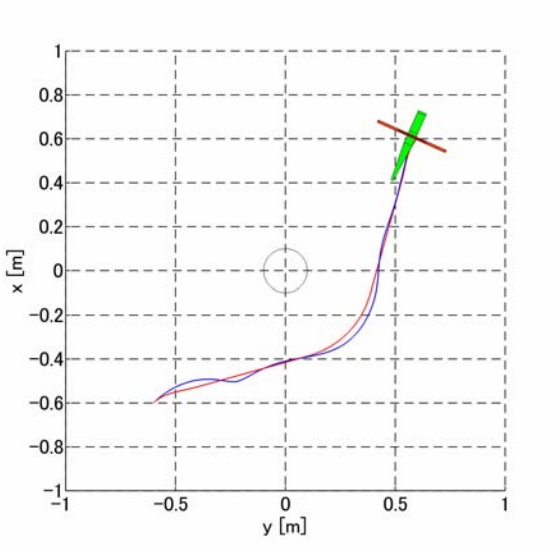

Figure 4. Simulation result of nose direction following tangential direction command.

III.B. Nose direction following the same direction

Let us consider the case in which an aircraft nose consistently keeps the same direction, i.e., maintains heading. Eq.(14) indicates reference values that the helicopter has to follow over time. Notice that the aircraft nose will constantly point at the upper right corner as the yaw angle is 45 degrees. The result for the simulation case is shown in Fig.5.

$$\begin{cases} x(t) & = & x_{cmd} \\ y(t) & = & y_{cmd} \\ \psi(t) & = & 45 \\ v_{Bx}(t) & = & \dfrac{s_f}{t_f}\cos(\psi_{cmd} - 45) \\ v_{By}(t) & = & \dfrac{s_f}{t_f}\sin(\psi_{cmd} - 45) \end{cases} \tag{14}$$

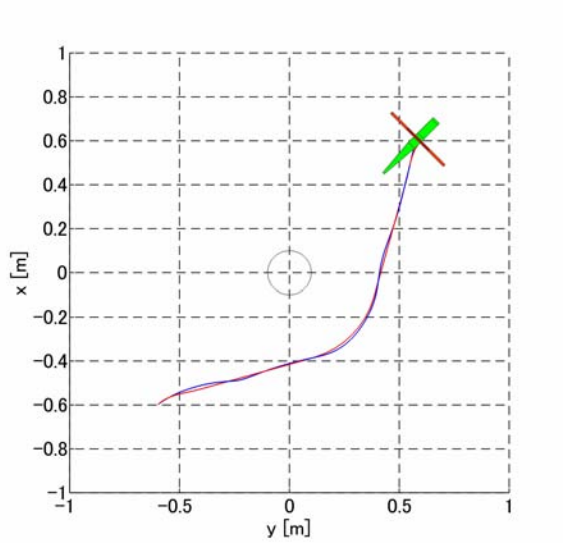

Figure 5. Simulation result of nose direction following the same direction.

III.C. Effect of flight time and nose orientation

In order to compare in a sole graphic the performance of the controller for the various nose-heading orientations, we introduce the cost function shown in Eq.(15) which is based on the integral of the control error. Let us assume that the error is the sum of the difference between the command value and the simulation value.

$$J_c = \frac{1}{s_f}\int_0^{t_f} \sqrt{(x - x_c)^2 + (y - y_c)^2 + (h - h_c)^2}\,dt \tag{15}$$

Cost J_c as a function of defined maximal flight time t_f is displayed in Fig.6. To show aircraft maneuverability, Fig.6 includes simulation case with $\psi = 45$ degrees and $\psi = 90$ degrees.

There are two noteworthy points about this figure. First, we can easily see that the cost decreases exponentially with increasing time. Indeed, it is evident that if our rotary-wing aircraft moves fast, the feedback controller will respond reasonably fast and lead to some overshoot behavior. Secondly, the cost is smaller when the helicopter keeps the same nose orientation. In addition to this, we can see that results with $\psi = 45$ degrees and $\psi = 90$ degrees share similar values. This fact demonstrates on one hand the incredible maneuverability of a rotary-wing aircraft and on the other, that keeping the same yaw angle helps the guidance controller as the helicopter does not have to change direction; hence, influencing other control variables.

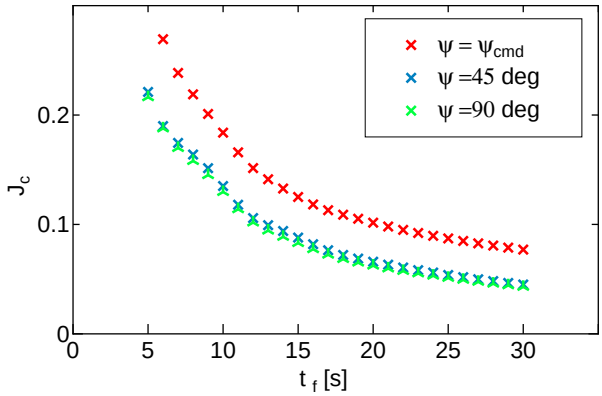

Figure 6. Cost J_c as a function of t_f

IV. Flight Experiment

In this last section, a guidance controller is developed and implemented using a simulated nonlinear model of the SCR UAV. In contrast with the above simulations, this section explores the implementation of optimal states variables applied to a real system. As we are now able to design and implement PID controllers to track an optimal trajectory generated from a nonlinear model, we can test a semi-autonomous flight of a small UAV in the indoor flight facility of the National Defense Academy (NDA) of Japan,[11]Fig.7.

Figure 7. Indoor flight facility in the Measurement and Control Laboratory of NDA.

IV.A. Results of two dimensional flight

Fig.8 and 9 show the results for a two-dimensional flight where the altitude of the vehicle is held constant. Again, as we previously pointed out in Fig.2 and 3, the environment model is limited to a simple cylindrical obstacle for efficiency and ease of simulation. The obstacle radius is equal to 0.1 m. In accordance with the helicopter length, the augmented obstacle radius used to find the optimal trajectory is equal to 0.4 m. Moreover, the helicopter depicted in the following figures is represented to scale for more clarity. Thus, the size on Fig.8 and 9 are proportional to the real size. Notice that, the UAV is flying at an altitude of 0.7 m to hover out of ground effect.

Even for this indoor flight, the UAV's motion varies due to the inherent feature of its nonlinear dynamics and/or wind disturbance caused by its rotor flow. From the flight results, the position error is approximately $\epsilon_R \leq 0.1$ m and the velocity error is approximately $\epsilon_V \leq 0.1$ m/s. Although there is no significant difference between both test cases, these tolerances are equivalent to that of the PID controlled flight.[11]

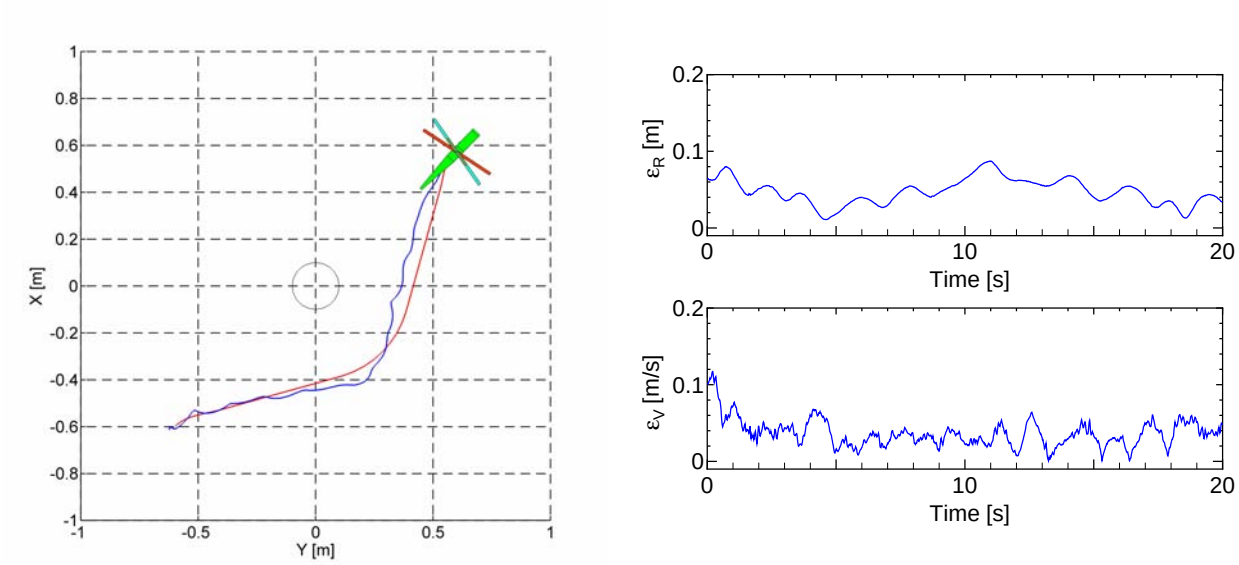

Figure 8. Following tangential direction command, trajectory, norm position error and norm velocity error.

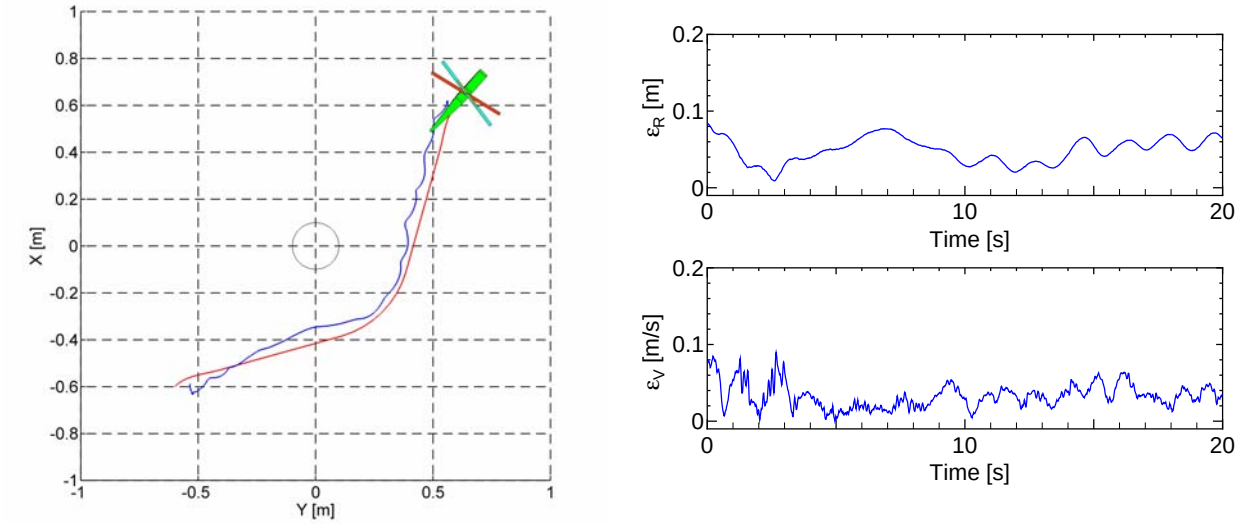

Figure 9. Following the same direction, trajectory, norm position error and norm velocity error.

IV.B. Result of three dimensional flight

In the previous section, the helicopter was able to avoid the obstacle in a preplanned environment while maintaining the same altitude. Since many applications for small UAVs require the ability to navigate in urban terrain at low altitude, 3D obstacle avoidance is paramount. Indeed UAVs must have the ability to plan trajectories that are free from collision with buildings, trees or unlevel ground.[33] In addition to this, it is worth noticing that following a preplanned 3D trajectory with pre-specified orientations is the logical stepping-stone test moving towards more autonomous UAV flight guidance and control. Therefore, the next step is to obviously check that the optimal control approach can be applied to 3D trajectories.

Fig.10-13 show the results for the 3D flight. Again, the tolerance is equivalent to that of the PID controlled hovering flight.[11] Obviously, uncertainties in position and velocity contribute to the tracking errors in addiiton to any descrapancies of excluding the vehicle dynamics in the kinematic path planning approach. However, the demonstrated errors of less than 0.1 m/s in velocity and 0.1 m in position deviation may be acceptable depending on application and/or mission requirements.[38]

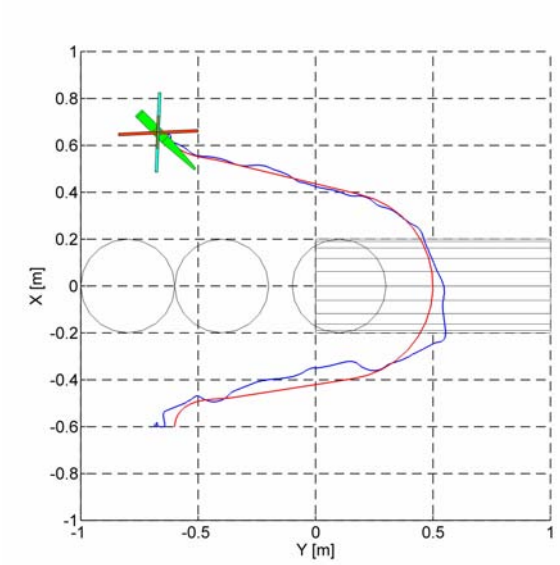

Figure 10. 3-dimensional trajectory tracking; x-y plane.

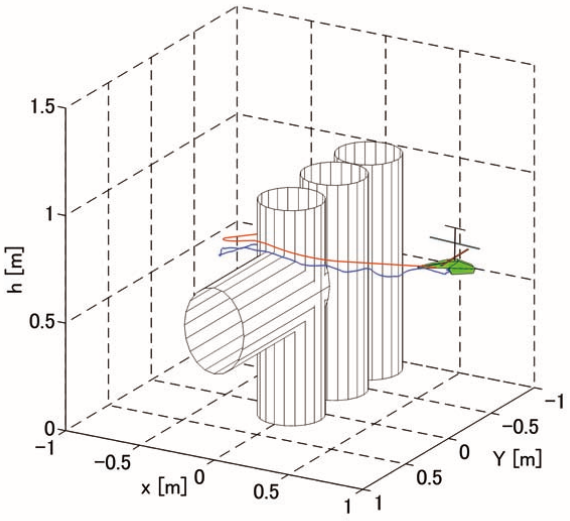

Figure 11. 3-dimensional trajectory tracking; xyh-plane.

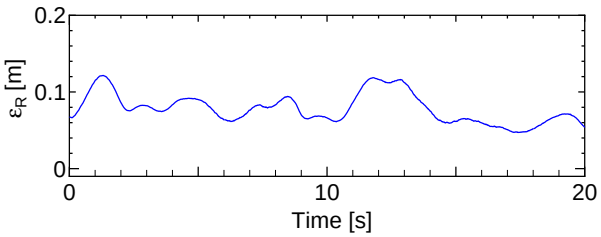

Figure 12. 3-dimensional trajectory tracking; position error.

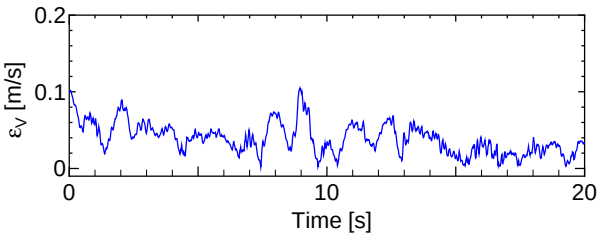

Figure 13. 3-dimensional trajectory tracking; velocity error.

V. Conclusions

This paper presented the results of a preliminary investigation into the adaptability of numerical optimal controls applied to a real UAV flight demonstration involving basic obstacle avoidance. As shown, the optimal path is applied as a reference command input to the SCR UAV tracking controller. With relatively little errors for the short-duration flights inside the NDA flight facility, this demo, albeit simplistic, validated the feasibility of the approach and is a mere stepping stone for further research. Future work will explore accounting for uncertainties and adding more realism (i.e. more fidelity) to the simplifications taken in this study.

Appendix

Nonlinear Dynamical Model of Single Coaxial UAV

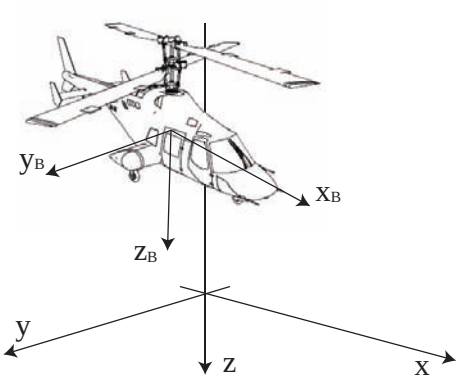

Figure 14. Coordinate System and Reference Frames of the Single Coaxial Rotor UAV.

The nonlinear dynamical model of the SCR UAV including stabilizer bar dynamics were adapted from the literature.[8,9] The state vector is $\boldsymbol{X} = [x\ y\ z\ v_{Bx}\ v_{By}\ v_{Bz}\ \phi\ \theta\ \psi\ p\ q\ r\ \alpha_S\ \beta_S\ \alpha_L\ \beta_L\ \Omega_U\ \Omega_L]^T$, where α_S and β_S are stabilizer angle, α_L and β_L are lower rotor angle, Ω_U and Ω_L are rotor angular rate. The control vector is $\boldsymbol{U} = [\delta_x\ \delta_y\ \delta_z\ \delta_\psi]$.

$$
\dot{\boldsymbol{X}}(t) = \begin{bmatrix}
v_{Bx}c\theta c\psi + v_{By}(s\phi s\theta c\psi - c\phi s\psi) + v_{Bz}(c\phi s\theta c\psi + s\phi s\psi) \\
v_{Bx}c\theta s\psi + v_{By}(s\phi s\theta s\psi + c\phi c\psi) + v_{Bz}(c\phi s\theta s\psi - s\phi c\psi) \\
-v_{Bx}s\theta + v_{By}s\phi c\theta + v_{Bz}c\phi c\theta \\
rv_{By} - qv_{Bz} - \frac{k_{fU}}{m}\Omega_U^2 \sin\alpha_U \cos\beta_U - \frac{k_{fL}}{m}\Omega_L^2 \sin\alpha_L \cos\beta_L - gs\theta \\
-rv_{Bx} + qv_{Bz} + \frac{k_{fU}}{m}\Omega_U^2 \sin\beta_U + \frac{k_{fL}}{m}\Omega_L^2 \sin\beta_L + gs\phi c\theta \\
qv_{Bx} - pv_{By} - \frac{k_{fU}}{m}\Omega_U^2 \cos\alpha_U \cos\beta_U - \frac{k_{fL}}{m}\Omega_L^2 \cos\alpha_L \cos\beta_L + gc\phi c\theta \\
p + (qs\phi + rc\phi)t\theta \\
qc\phi - rs\phi \\
\frac{qs\phi + rc\phi}{c\theta} \\
\frac{J_y - J_z}{J_x}qr - \frac{1}{J_x}(z_{HU}k_{fU}\Omega_U^2 \sin\beta_U + z_{HL}k_{fL}\Omega_L^2 \sin\beta_L) \\
\frac{J_z - J_x}{J_y}rp - \frac{1}{J_y}(z_{HU}k_{fU}\Omega_U^2 \sin\alpha_U \cos\beta_U + z_{HL}k_{fL}\Omega_L^2 \sin\alpha_L \cos\beta_L) \\
\frac{J_x - J_y}{J_z}pq + \frac{1}{J_z}(k_{mU}\omega_U^2 - k_{mL}\omega_L^2) \\
\frac{1}{T_S}(\theta - \alpha_S) \\
\frac{1}{T_S}(\phi - \beta_S) \\
\frac{1}{T_{fL}}(K_x\delta_x - \alpha_L) \\
\frac{1}{T_{fL}}(K_y\delta_y - \beta_L) \\
m_1\delta_z + m_2\delta_\psi - m_3\Omega_U \\
m_1\delta_z - m_2\delta_\psi - m_3\Omega_L
\end{bmatrix}
$$

References

[1]Kendoul,F., Lara,D., Fantoni-Coichot,I. and Lozano, R., "Real-Time Nonlinear Embedded Control for an Autonomous Quadrotor Helicopter", *Journal of Guidance, Control, and Dynamics*, Vol.30, No.4, 2007, pp.1049-1061.

[2]Pollini,L. and Metrangolo,A., "Simulation and Robust Backstepping Control of a Quadrotor Aircraft", *AIAA Guidance, Navigation and Control Conference*, AIAA 2008-6363, 2008.

[3]Hoffmann,G.M. and Waslander,S.L., "Quadrotor Helicopter Trajectory Tracking Control", *AIAA Guidance, Navigation and Control Conference*, AIAA 2008-7410, 2008.

[4]Michini,B. and How,J.P., "$\mathcal{L}_1$Adaptive Control for Indoor Autonomous Vehicles: Design Process and Flight Testing", *AIAA Guidance, Navigation and Control Conference*, AIAA 2009-5754, 2009.

[5]Zhao,L. and Murthy, V.R., "Optimal Controller for an Autonomous Helicopter in Hovering and Forward Flight", *AIAA Aerospace Sciences Meeting Including The New Horizons Forum and Aerospace Exposition*, AIAA 2009-57, 2009.

[6]Karpenko,M., Sekhavat,S., Park, J. and Ross, I.M., "Closed-Loop Optimal Guidance and Control of Quadrotor Unmanned Aerial Vehicle", *AIAA Guidance, Navigation and Control Conference*, AIAA 2010-8051, 2010.

[7]Lupashin,S., Schollig,A., Sherback,M. and D'Andrea,R., "A Simple Learning Strategy for High-Speed Quadrocopter Multi-Flips", *Proc. of the IEEE Int. Conf. on Robotics and Automation*,2010.

[8]Schafroth,D., Bermes,C., Bouabdallah,S. and Siegwart, R., "Modeling, System Identification and Robust Control of a Coaxial Micro Helicopter", *Control Engineering Practice*, Vol.18, No.7, 2010,pp.700-711.

[9]Mukherjee,P. and Waslander, S., Modeling and Multivariable Control Techniques for Small Coaxial Helicopter, *AIAA Guidance, Navigation and Control Conference*, AIAA 2011-6545, 2011.

[10]Harada, M. and Bollino K., "Minimum-Time Circling Flight of a Triarm Coaxial Rotor UAV", *AIAA Guidance, Navigation and Control Conference*, AIAA-2011-6718, 2011.

[11]Harada, M., Ito, M., Nagata, H. and Bollino K., "Minimum-Time Hover-to-Hover Maneuver of a Single Coaxial Rotor UAV : Example and Experimental Results", *AIAA Guidance, Navigation and Control Conference*, AIAA 2012-4836, 2012.

[12]Li, T., Zhang, Y. and Gordon, B. W., "Investigation, Flight Testing and Comparsion of Three Nonlinear Control Techniques with Application to a Quadrotor Unmanned Aerial Vehicle", *AIAA Guidance, Navigation and Control Conference*, AIAA 2012-4916, 2012.

[13]How,J.P., Betheke,B.,Frank,A.,Dale,D. and Vian,J., "Real-Time Indoor Autonomous Vehicle Test Environment", *IEEE Control Systems Magazine*, 2008, pp.51-64.

[14]Bryson,A.E., and Ho,Y.C., "Applied Optimal Control", *Taylor& Francis*,Levittown,1975.

[15]Ben-Asher,J.Z., "Optimal Control Theory with Aerospace Applications", *AIAA Education Series*, Virginia, 2010.

[16]Betts, J.T., "Survey of Numerical Methods for Trajectory Optimization", *Journal of Guidance, Control, and Dynamics*, Vol.21, No.2, 1998, pp.193-207.

[17]Elnagar,G., Kazemi,A., and Razzaghi, M., "The Pseudospectral Legendre Method for Discretizing Optimal Control Problems", *IEEE Transactions on Automatic Control*,**40**-10(1995),1793-1796.

[18]Fahroo,F.,and Ross,I.M., "Costate Estimation by a Legendre Pseudospectral Method", *Journal of Guidance, Control, and Dynamics*, Vol.24, No.2, 2001, pp.270-277.

[19]Ueno,S., Watanabe,R., Mitsui,M. and Ishimoto, S., "Optimal Guidance and Control Law of Future Space Transportation System in an Emergency Case", *Asia-Pacific International Symposium on Aerospace Technology*, JSASS-2009-5607, 2009, pp.592-595.

[20]Mayne D. Q., Ralings J. B., Rao C. V. and Scokaert P. O. M., "Constrained Model Predictive Control: Stability and Optimality", *Automatica*, Vol. 36, No. ,2000, pp.789-814.

[21]Ross,I.M., Sekhavat,P.,Fleming,A. and Gong,Q., "Optimal Feedback Control: Foundations, Examples, and Experimental Results for a New Approach", *Journal of Guidance, Control, and Dynamics*, Vol.31, No.2, 2008, pp.307-321.

[22]Bollino, K., Oppenheimer M., and Doman, D., "Optimal Guidance Command Generation and Tracking for Reusable Launch Vehicle Reentry", *AIAA Guidance, Navigation and Control Conference*, AIAA 2006-6691, 2006.

[23]A.E. Bryson: Optimal Control -1950 to 1985, IEEE Control Systems, **16**-3, 26/33(1996)

[24]Tsuchiya,T., Ishii,H., Uchida,J. and Ikaida, H., "Flight Trajectory Optimization to Minimize Ground Noise in Helicopter Landing Approach", *Journal of Guidance, Control, and Dynamics*, Vol.32, No.2, 2009, pp.605-615.

[25]Suzuki,S. Komatsu, Y., Yonezawa, S., Masui, K. and Tomita,H., "Online Four-Dimensional Flight Trajectory Search and its Flight Testing", *AIAA Guidance, Navigation and Control Conference*, AIAA 2005-6475, 2005.

[26]Tsuchiya,T., Miwa,M. and Suzuki, S., "Real-Time Flight Trajectory Optimization and Its Verification in Flight", *Journal of Aircraft*, Vol.46, No.4, 2009, pp.1468-1470.

[27]Evans,C.A., Robinson, J.A., Tate-Brown,J., Thummm,T., Crespo-Richey,J., Baumann, D. and Rhatigan J., "International Space Station Science Research Accomplishments During the Assembly Years: An Analysis of Results from 2000-2008", NASA-TP-2009-213146-REVISION A.

[28]Bedrossian,N.,Bhatt,S.,Lammmers, M. and Nguyen,L., "Zero Propellant Maneuver Flight Results for 180 degree ISS Rotation", NASA-CP-2007-214158.

[29]Karpenko, M., Bhatt, S., Bedrossian,N., Fleming, A. and Ross, I. M., "First Flight Results on Time-Optimal Spacecraft Slews", *Journal of Guidance, Control, and Dynamics*, Vol.35, No.2, 2012, pp.367-376.

[30]Lewis, L. R., "Rapid Motion Planning and Autonomous Obstacle Avoidance for Unmanned Vehicles", *Master Thesis, Naval Postgraduate School*, 2006.

[31]Bollino, K., and Lewis, L. R., "Optimal Path Planning and Control of Tactical Unmanned Aerial Vehicles in Urban Environments", *Proc. of AUVSI's Unmanned Systems North America 2007 Conference*, AIAA 2008-7134, 2007.

[32]Hurni, M., Sekhavat, P., and Ross, I.M., "Autonomous Trajectory Planning Using Real-Time Information Updates", *AIAA Guidance, Navigation and Control Conference*, AIAA 2008-6305, 2008.

[33]Bollino K., and Lewis, L.R., "Collision-free Multi-UAV Optimal Path Planning and Cooperative Control for Tractical Applications", *AIAA Guidance, Navigation and Control Conference*, AIAA 2008-7134, 2008.

[34]Cichella, V., Xargay, E., Dobrokhodov, V., Kaminer, I., Pascoal, A. M. and Hovakimyan, N., "Geometric 3D Path-Following Control for a Fixed-Wing UAV on SO(3)", *AIAA Guidance, Navigation and Control Conference*, AIAA 2011-6415, 2011.

[35]Julier,S. and Uhlmann, J.K., Unscented Filtering and Nonlinear Estimation, *Proceedings of the IEEE*, Vol.92, No.3, 2004, pp.401-402.

[36]Jategaonkar R. V., "Flight Vehicle System Identification: A Time Domain Methodology", *AIAA Progress in Astronautics and Aeronautics*, AIAA, 2006.

[37]Harada, M., "Direct Trajectory Optimization by a Jacobi Pseudospectral Method with the Weights of High-Order Gauss-Lobatto Forumulae", *Transactions of Japan Society of Mechanical Engineers*, Series C, Vol.73, No.728, 2007, pp.119-124. (in Japanese)

[38]Japan UAV Association, "Safety Standards for Commercial-Use, Unmanned, Rotary-Wing Aircraft in Uninhabited Areas", *Japan UAV Association*, http://www.juav.org/, 2005.